Applied Physics Express 6 (2013) 103002
http://dx.doi.org/10.7567/APEX.6.103002

Electromagnetic Field Enhancement and Its Application in Spin Rectification

Fuchun Xi[1], Lijian Zhang[1], Jie Xu[1], Lei Fu[2], Yongsheng Gui[2], Canming Hu[2], Lei Zhou[1], Shan Qiao[1], and Zhenghua An[1]*

[1]*Laboratory of Advanced Materials, State Key Laboratory of Surface Physics and Key Laboratory of Micro and Nano Photonic Structures (Ministry of Education), Fudan University, Shanghai 200433, China*
[2]*Department of Physics and Astronomy, University of Manitoba, Winnipeg R3T 2N2, Canada*
E-mail: anzhenghua@fudan.edu.cn

Received July 1, 2013; accepted August 30, 2013; published online September 18, 2013

A subwavelength antenna, which has the capability to enhance both the microwave electric and magnetic fields, is proposed for use in spintronic devices. The geometric resonance of the microwave electric and magnetic fields in the antenna are determined by spintronic techniques, and are in remarkable agreement with measurements taken using a vector network analyzer and simulations based on the finite-difference time-domain method. Our simulations predict that the performance of a spin dynamo may be improved by three orders of magnitude if properly integrated with this antenna on-chip. © 2013 The Japan Society of Applied Physics

It has been shown that spintronic devices based on ferromagnetic materials under microwave radiation can produce a dc voltage and/or current via the spin rectification effect, which is linearly proportional to the power of the microwave.[1–7] Owing to the high conversion efficiency of this microwave rectification, the electrical detection technique has become a powerful tool to investigate spin dynamics in ferromagnetic materials and structures as well as to image microwave spatial distribution.[8–10] The microwave power sensitivity in spintronic devices, which is characterized by the ratio between the produced dc voltage and the incident microwave power, can be as high as a few 100 mV/mW.[11,12] Therefore, such spintronic devices can be fed by means of wireless power transmission, which can act as a power supply for sensors and microprocessors without an on-board battery. Although the sensitivity of spintronic devices cannot yet compete with existing microwave detection technologies (such as passive semiconductor Schottky-diode microwave detectors with a power sensitivity of about 1000 mV/mW), at microwatt levels, Schottky diodes become very inefficient for wireless power transmission because their zero bias resistance (on the order of a few kΩ) is too large.[13,14] In this case, the converted dc power is mainly consumed by the diode itself rather than used to power other devices. In contrast, the zero bias resistance of spintronic devices can be easily adjusted by tuning their dimensions; consequently, they are a promising alternative for ambient microwave power harvesting.[14]

Differing from any conventional semiconductor microwave sensors, the spin dynamo[6] is sensitive not only to the electric field (*e*-field) of microwaves but also to their magnetic field (*h*-field).[15,16] Consequently, the design of an antenna integrated with a spin dynamo for practical applications should take into account the microwave *h*-field as well as the microwave *e*-field utilized in conventional antennas. Based on the knowledge that a bowtie antenna[17,18] has the capability to enhance the *e*-field by decreasing its gap, while a diabolo antenna[19] has the capability to enhance the *h*-field by narrowing its central strip line, we report on a subwavelength antenna (SA) that combines the bowtie-type and diabolo-type antennas together to simultaneously enhance both *e*-field and *h*-field in its central near-field range. A spin dynamo has been used to verify the performance of the enhancement of such an antenna for both *e*- and *h*-fields.

As shown in the inset of Fig. 1(a), the antenna has a dimension of $5 \times 5\,\mathrm{mm}^2$ ($l = 5\,\mathrm{mm}$) in the x–z plane, and includes several copper lines with thickness of $t = 500\,\mathrm{nm}$ and width of $w = 0.25\,\mathrm{mm}$ deposited on a 50-μm-thick poly(ethylene terephthalate) (PET) substrate. Two pairs of copper strips form two gaps of $g = 0.9\,\mathrm{mm}$ near the centre of the antenna. From a technical point of view, the antenna is similar to an LCR parallel circuit consisting of a resistor of R, an inductor of L and a capacitor of C with a resistance in series with the inductor, which has an intrinsic resonance frequency $\omega = \sqrt{1/LC - R^2/4L^2}$. To understand the performance of the antenna, the finite-difference time-domain method (FDTD)[20] is used for simulation. Given the dielectric constant $\epsilon_r = 2.9$ for the PET substrate, an intrinsic resonance frequency of 8.84 GHz is found. By adjusting the dimensions of the antenna, this frequency changes. As shown in Fig. 1(a), the enhancements ζ [$\zeta = (A^{\mathrm{SA}} - A^{\mathrm{in}})/A^{\mathrm{in}}$, where A^{SA} is the transmitted field amplitude near the antenna and A^{in} is the amplitude of incident field] of both the *e*-field and the *h*-field are calculated for a point distance of $y = 1.5\,\mathrm{mm}$ away from the centre of the antenna (the origin point of the x–y–z coordinate system). Note that this definition is different from plasmonic community where $(A^{\mathrm{SA}^2}/A^{\mathrm{in}^2})$ is typically defined to be the enhancement factor.[19] The enhancement of the *e*-field is attributed to the gaps beside the central strip, while the enhancement of the *h*-field is generated by the focused microwave current flowing in the central strip.

Conventionally, the distribution of the microwave *e*-field can be precisely detected using a vector network analyser (VNA) and a near-field probe. This measurement has been carried out in a setup shown in the inset of Fig. 1(c), where an X-band (8–12 GHz) horn waveguide connected to the port 1 of VNA is used to emit microwaves, and a near-field probe connected to the port 2 of VNA is used to receive the microwaves transmitted from the antenna. The near-field probe is made by cutting a semirigid coaxial cable (oriented along the y-direction) so that a roughly 2-mm-long piece of its core wire remains out of the shielding; it is then bent forward in the z-direction (the polarization direction of the *e*-field emitted from the centre of the horn waveguide). This probe is aligned with the centre of the waveguide, and the antenna between them is placed on a computer-controlled positioner that can move in the x-, y-, and z-directions with a resolution of 5 μm and a travel range of 50 mm.

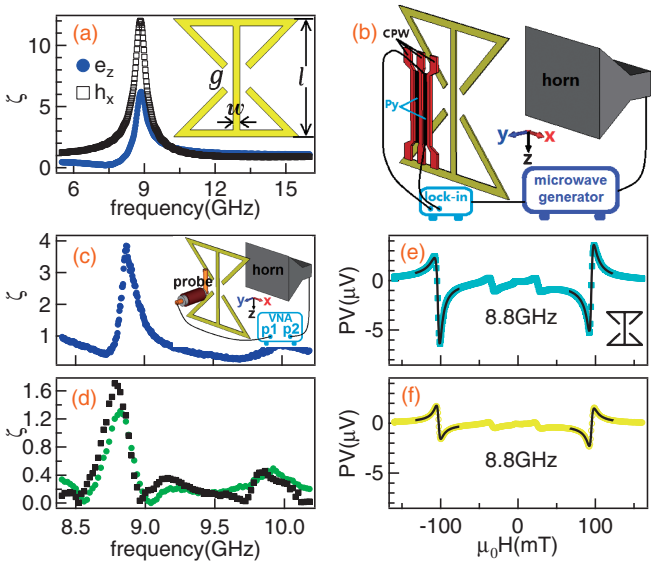

Fig. 1. (a) Simulated enhancements of e_z (solid circles) and h_x (open squares) as functions of microwave frequency. The schematic structure of the antenna is shown in the inset. (b) Diagram of the experimental setup measuring the microwave photovoltage (PV) using a spin dynamo. (c) ζ as a function of the microwave frequency extracted from a VNA measurement. The inset shows the diagram of experimental setup measuring e-field using a near-field probe. (d) Same as (c) but via a microwave PV measurement using a spin dynamo, the solid circles and solid squares correspond to the PV amplitude of FMRs at positive and negative magnetic field biases, respectively. Typical PV spectra at 8.8 GHz are plotted in (e) and (f) for cases with and without the antenna, respectively. Solid black lines are the calculated line shape of the FMR according to Eq. (1) and solid light blue and yellow symbols are experimental data.

A typical measurement result for a distance of $y = 0.5$ mm between the probe and the antenna is shown in Fig. 1(c), where the enhancement $\zeta = |S_{21}^{\mathrm{SA}} - S_{21}^{\mathrm{ref}}|/S_{21}^{\mathrm{ref}}$ denotes the ratio of the measured S_{21} parameters for the cases with the antenna (S_{21}^{SA}) and without the antenna (S_{21}^{ref}). The maximum value of ζ is at a frequency of 8.87 GHz (the corresponding wavelength in vacuum is 34 mm), which is close to the simulated result of 8.84 GHz. To rule out the possibility that this resonant structure is due to coupling between the antenna and the probe, we have carried out two independent experiments. In the first experiment, we have moved the antenna in x–z plane and measured ζ as a function of frequency (not shown). The results indicate an almost identical resonant frequency, although the amplitude of ζ varied significantly with position (the overall tendence is that ζ is large when the probe is near the central gap region and decreases when the probe is moved faraway). Additionally, the E_x and E_y (electric field components along x- and y-directions) were measured with the bare core wire of semirigid coaxial cable bending forward in x- and y-directions, respectively. The E_x is so small that it's difficult to determine the resonant frequency. The E_y is strong and it shows the same resonant frequency as E_z.

In the second measurement, a spin dynamo was used to probe this resonant effect. The main component of such a spin dynamo is a permalloy ($Ni_{80}Fe_{20}$, Py) microstrip (typically 2.45 mm × 20 μm × 80 nm). The Py strip is along the z-direction (the polarization direction of the microwave e-field), and the width of the Py is along the x-direction. The spin dynamo can convert the microwaves into a dc voltage (PV) according to the spin rectification effect,[6] i.e., $\mathrm{PV} \propto \langle j \cdot m \rangle$, where j is the current induced by the microwave e-field, m is the nonequilibrium magnetization driven by the microwave h-field, and $\langle \cdots \rangle$ denotes the time average. Obviously, the amplitude of m reaches a maximum value at the ferromagnetic resonance (FMR) and, hence, the PV spectra in Figs. 1(e) and 1(f) show such a resonant effect. As detailed in the discussion of Ref. 8, because of the relative phase between the microwave e- and h-field, PV spectra near FMR show a combination of Lorenz and dispersive line shapes given by

$$\mathrm{PV} = A_{\mathrm{L}} \frac{\Delta H^2}{(H - H_0)^2 + \Delta H^2} + A_{\mathrm{D}} \frac{\Delta H (H - H_0)}{(H - H_0)^2 + \Delta H^2}, \quad (1)$$

where H_0 is the resonant magnetic field, ΔH is the linewidth, H is the external magnetic field, and A_{L} and A_{D} are the amplitudes for the Lorenz and dispersive components, respectively. To measure PV spectra detected by the spin dynamo, the experiment setup is shown in Fig. 1(b) that is similar to the one depicted in the inset of Fig. 1(c). But the VNA is no longer used, and the probe is replaced by the spin dynamo and the horn waveguide is connected to a microwave generator where the output microwave power was amplitude-modulated by a square wave, and a lock-in amplifier triggered by such a squared wave was employed to detect the rectified PV signal. The external magnetic field was oriented 45° with respect to the z-direction in the x–z plane and the antenna was placed 1.5 mm away from the spin dynamo. A typical PV spectrum at 8.8 GHz is plotted in Fig. 1(e), where the FMR line shape can be well fitted by Eq. (1) with a resonant amplitude of $\mathrm{PV}^{\mathrm{SA}} = \sqrt{A_{\mathrm{L}}^2 + A_{\mathrm{D}}^2}$. The dispersion of the FMR (not shown) follows Kittel's formula $\omega = \gamma\sqrt{H_0(H_0 + M_0)}$ with $\gamma/2\pi\mu_0 = 29\,\mathrm{GHz/T}$ and a saturation magnetization $\mu_0 M_0 = 1.1\,\mathrm{T}$.

For a systematic comparison, we have also measured the PV spectrum for the situation without the antenna. As shown in Fig. 1(f), the FMR line shape is also well fitted by Eq. (1) with an amplitude of $\mathrm{PV}^{\mathrm{ref}}$. Thus, the enhancement $\zeta = |\mathrm{PV}^{\mathrm{SA}} - \mathrm{PV}^{\mathrm{ref}}|/\mathrm{PV}^{\mathrm{ref}}$ due to the antenna is shown in Fig. 1(d). The solid circles and solid squares correspond to a positive and negative H biases, respectively. It clearly shows a resonant-type enhancement near 8.78 and 8.82 GHz for positive and negative H biases, respectively. These resonant positions are in excellent agreement with both the simulation result and the measurements performed via VNA, which clearly indicates the intrinsic geometrical resonance of the antenna. It should also be noted that the enhancement of the PV signal is due to the enhancement of the microwave field, and hence, can be observed not only from the PV near FMR, but also from the PV near spin wave resonances (resonances at fields below FMR) as well as nonresonant PV in the vicinity of $H = 0$.[9,10]

So far, the near-field enhancement of the microwave e-field is clearly seen using a near-field probe and a VNA. However, from a single PV spectrum, we cannot conclude the enhancement effect of the microwave h-field from the measured PV signal in a spin dynamo since PV is in general a product of e-field and h-field. In order to separate the

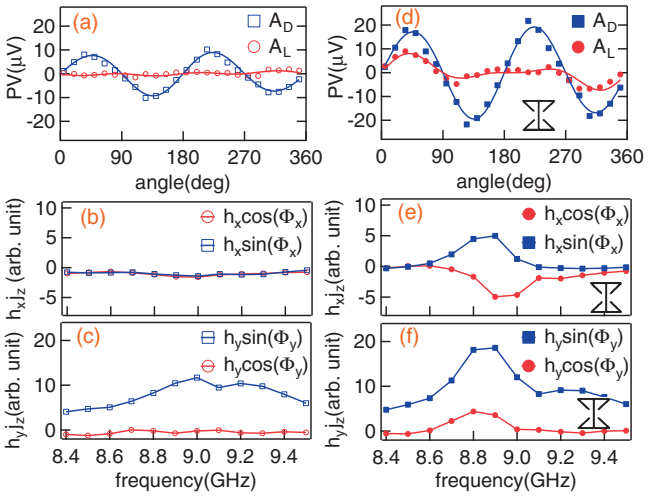

Fig. 2. Separated Lorentz and dispersive line shapes (circles and squares, respectively) as a function of θ from a fit to Eq. (1) at $\omega/2\pi = 8.8$ GHz for cases without (a) and with (d) the antenna. (b) and (c) are the h_y and h_x fields deduced from θ-dependent Lorenz and Dispersive components at various frequencies for a situation without the antenna; (e) and (f) are ones with the antenna.

contributions caused by the microwave e-field and the microwave h-field, and hence, demonstrate the near-field enhancement of the microwave h-field by the antenna, we have measured the angular-dependent PV spectra by varying the orientation of the external applied H-field. In such an experiment, the amplitudes A_L and A_D of the Lorentz and dispersive line-shape contributions to the PV signal can be expressed as[8,9]

$$A_L = \Delta R j_z \sin(2\theta)[-A_{xx}h_x \sin(\Phi_x)\cos(\theta) + A_{xx}h_z \sin(\Phi_z)\sin(\theta) - A_{xy}h_y \cos(\Phi_y)]/2M_0, \quad (2)$$

$$A_D = \Delta R j_z \sin(2\theta)[A_{xx}h_x \cos(\Phi_x)\cos(\theta) - A_{xx}h_z \cos(\Phi_z)\sin(\theta) - A_{xy}h_y \sin(\Phi_y)]/2M_0, \quad (3)$$

where Φ_x, Φ_y, and Φ_z are the relative phases between the microwave electric and magnetic fields in the x-, y-, and z-directions, respectively, θ is the angle between H and the permalloy strip (z-direction) in the xz plane, ΔR is the resistance change due to the AMR effect, j_z is the rf current along the Py strip (which satisfies $j_z = \sigma e_z$), e_z is the amplitude of the z component of the microwave e-field emitted from the horn waveguide, and σ is the conductivity of Py. The prefactors A_{xx}, A_{xy}, and A_{yy} are real numbers, which are related to the Py properties.[8,9]

The amplitudes A_L and A_D in Eqs. (2) and (3), respectively, of the Lorentz and dispersive line-shape contributions, show a complex dependence on each component of the microwave h-field as well as on its relative phase. However, the fingerprints of $A_L, A_D \propto \sin(2\theta)\cos\theta$ for h_x $A_L, A_D \propto \sin(2\theta)$ for h_y and $A_L, A_D \propto \sin(2\theta)\sin\theta$ for h_z allow the contributions to A_L and A_D from h_x, h_y, and h_z to be easily separated.

This separation is done using the Lorentz and dispersive amplitudes determined from a fit to the FMR at $\omega/2\pi = 8.8$ GHz, which are plotted as a function of θ in Figs. 2(a) and 2(d) for cases without and with the SA, respectively. A fit using Eqs. (2) and (3) allows the contributions from each of the h_x, h_y, and h_z fields to be separated based on their different contributions to the θ dependence of the line shape. The results of the fit for a set of frequencies have been plotted in Figs. 2(b)–2(f), where $h\cos(\Phi)$ and $h\sin(\Phi)$ indicate the components of the microwave h-fields in-phase and out-of-phase with respect to j_z due to the existence of a nonzero relative phase. Without the SA, a fairly flat dependence of the microwave frequency [Figs. 2(b) and 2(c)] is observed; with the SA, a clear resonant (8.8 GHz) structure is observed for both the in-phase ($h\cos\Phi$) and out-of-phase ($h\sin\Phi$) components of h_x and h_y in Figs. 2(e) and 2(f) because of the geometrical resonance of the antenna.

In contrast to the VNA measurement, which can only detect enhancement of the microwave e-field, the spin dynamo has the capability to detect the enhancement of both the microwave e- and h-field by carefully checking the deduced h-vector. The h_z component (not shown) is at least one order of magnitude smaller than the h_x and h_y components. This observation is in agreement with the waveguide theory that the h_z-field should not exist for transverse electric (TE_{10}) waves emitted from a horn waveguide. Following such a rule, one can also expect a dominant h_x field near the centre of a horn waveguide. Indeed, such an h-vector has been directly measured via the electrical detection technique.[15] However, Fig. 2 clearly shows a dominant h_y component. Note that in the spin dynamo, the Py microstrip is inserted in the middle of the slot between ground and signal strips of a coplanar waveguide (CPW).[6] The microwaves radiated from the horn waveguide result in a microwave current flowing through the highly conductive CPW (along the z-direction) and, hence, a microwave h-field polarized along the y-direction is produced according to the Biot-Savart law in the neighbouring Py strip (a distance of less than 100 μm away). Because the measured $h_y j_z$ component is solely due to the contribution from the microwave e-field as shown in the discussion above, the enhancement of the e-field $\zeta_e = j_z^{SA}/j_z^{ref} - 1$ to 0.5 at $\omega/2\pi = 8.8$ GHz can be estimated from the ratio of $h_y^{SA} j_z^{SA}/h_y^{ref} j_z^{ref} \sim (j_z^{SA}/j_z^{ref})^2 = 2.26$ shown in Figs. 2(c) and 2(f). We can further estimate the enhancement of the h-field $\zeta_h = h_x^{SA}/h_x^{ref} - 1$ to 1.04 from the ratio of $h_x^{SA} j_z^{SA}/h_x^{ref} j_z^{ref} \sim 3.05$ shown in Figs. 2(b) and 2(e).

For practical applications, the antenna can be integrated with a spin dynamo on-chip, which can significantly enhance the performance of the spin dynamo according to the simulation using the FDTD method. In our simulation, the microwave source is a plane wave, which propagates along the y-direction, and the polarizations of the e-field and h-field are along the z- and x-directions, respectively. Figure 3 shows calculated enhancements for electric and magnetic fields at an xz plane distance of 200 μm away from the SA ($y = 200$ μm), which indicates a maximum value of about 40 for the e_z-field and 120 for the h_x-field. The strongest e_z-field is located at the two gaps in the SA, while the strongest h_x-field is located above the central strip of the SA because all the electric current must flow through it, as shown in the right bottom inset of Fig. 3(b). If a spin dynamo is placed near the centre of the SA at a distance of about $y \sim 200$ μm, the resulting PV could be 2000 times larger. This enhancement factor (2000) is readily larger than the area enhancement [$5000^2/(20 \times 2450) = 500$]. We also calculate the PV through simulation in the plane

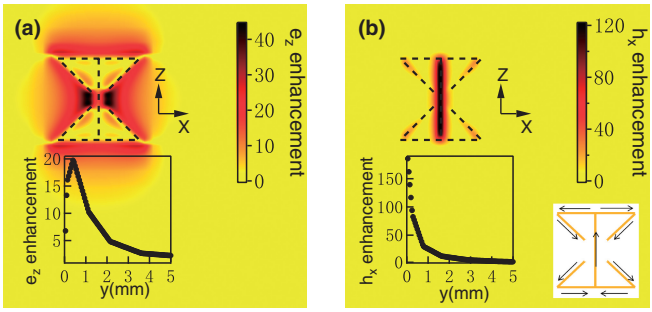

Fig. 3. (a) Two-dimensional distribution of the electric field enhancement (e_z) at $y = 200\,\mu m$, i.e., an xz plane located 200 μm away from the SA. The inset plots e_z as a function of y when $x = z = 0$. (b) Two-dimensional distribution of the magnetic field enhancement (h_x) at $y = 200\,\mu m$. The left inset shows h_x as a function of y for $x = z = 0$, and the right inset shows the current flow at the resonant state. The dashed contour of SA is over-layed in the figures as an aid to the reader.

of $y = 1.5\,mm$, and the resultant PV is about 30 times larger than the experimental one. The deviation between simulated and measured PV (and also electric and magnetic field enhancement) can be attributed to several reasons: First, the CPW structure is not yet optimized for SA antenna and therefore the large impedance mismatch exists between SA and the spin dynamo. Second, the substrate and electrodes and so on may influence the resonant property of the antenna. Third, the interaction between spin-dynamo and the antenna may alter the resonant mode property. These factors have not yet been considered in the simulation. In addition, the structural imperfection in device fabrication may also contribute to the deviation.

In the microwave rectification field, semiconductor diode is very competitive, however, the large zero-bias resistance restricts the lower power limit.[14] With the resonant nature which is efficient for field enhancement, our SA antenna should also be helpful for semiconductor diode rectifying, and the practical effect needs to be demonstrated experimentally.

In summary, a subwavelength SA has been fabricated for microwave applications in spintronic devices, which are sensitive to both microwave *e*- and *h*-field, in contrast to any conventional antenna. The resonant frequency of the antenna is measured by a near-field probe and a spin dynamo, and the results agree well with the simulation. The enhancement of both the microwave *e*- and *h*-field has been directly measured via a spin dynamo. It has been calculated that the performance of a spin dynamo can be improved by three orders of magnitude by integrating it with an SA. This effect implies a promising alternative for ambient microwave power harvesting via spintronic technique. Our work may pave a way to realize practical opto-spintronics.

Acknowledgments We would like to thank L. H. Bai for discussions. This work was jointly supported by the National Basic Research Program of China Grant No. 2009CB929300, the NSFC Contract Nos. 10804019/11174055/60990321, Shanghai Science and Technology Committee Contract No. 09dj1400103, the fund of graduate school of Fudan University for short-term international visit of doctoral student, NSERC, CFI, CBCF, and URGP grants.

1) H. J. Juretschke: J. Appl. Phys. **31** (1960) 1401.
2) W. G. Egan and H. J. Juretschke: J. Appl. Phys. **34** (1963) 1477.
3) A. Azevedo, L. H. Vilela Leão, R. L. Rodriguez-Suarez, A. B. Oliveira, and S. M. Rezende: J. Appl. Phys. **97** (2005) 10C715.
4) A. A. Tulapurkar, Y. Suzuki, A. Fukushima, H. Kubota, H. Maehara, K. Tsunekawa, D. D. Djayaprawira, N. Watanabe, and S. Yuasa: Nature (London) **438** (2005) 339.
5) J. C. Sankey, P. M. Braganca, A. G. F. Garcia, I. N. Krivorotov, R. A. Buhrman, and D. C. Ralph: Phys. Rev. Lett. **96** (2006) 227601.
6) Y. S. Gui, N. Mecking, X. Zhou, G. Williams, and C.-M. Hu: Phys. Rev. Lett. **98** (2007) 107602.
7) A. Yamaguchi, H. Miyajima, T. Ono, Y. Suzuki, S. Yuasa, A. Tulapurkar, and Y. Nakatani: Appl. Phys. Lett. **90** (2007) 182507.
8) M. Harder, Z. X. Cao, Y. S. Gui, X. L. Fan, and C.-M. Hu: Phys. Rev. B **84** (2011) 054423.
9) Y. S. Gui, L. H. Bai, and C. M. Hu: Sci. China Phys. Mech. Astron. **56** (2013) 124.
10) Z. X. Cao, W. Lu, L. Fu, Y. S. Gui, and C.-M. Hu: Appl. Phys. A **111** (2013) 329.
11) C. Wang, Y.-T. Cui, J. Z. Sun, J. A. Katine, R. A. Buhrman, and D. C. Ralph: J. Appl. Phys. **106** (2009) 053905.
12) S. Ishibashi, T. Seki, T. Nozaki, H. Kubota, S. Yakata, A. Fukushima, S. Yuasa, H. Maehara, K. Tsunekawa, D. D. Djayaprawira, and Y. Suzuki: Appl. Phys. Express **3** (2010) 073001.
13) J. A. Hagerty, F. B. Helmbrecht, W. H. McCalpin, R. Zane, and Z. B. Popovic: IEEE Trans. Microwave Theory Tech. **52** (2004) 1014.
14) S. Hemour, D. Houssameddine, R. Whig, J. M. Slaughter, K. Nagel, S. Aggarwal, Y. S. Gui, C.-M. Hu, and K. Wu: Microwave IEEE MTT-S Int. Symp. Dig. (MTT), 2012.
15) L. H. Bai, Y. S. Gui, A. Wirthmann, E. Recksiedler, N. Mecking, C.-M. Hu, Z. H. Chen, and S. C. Shen: Appl. Phys. Lett. **92** (2008) 032504.
16) X. Fan, R. Cao, T. Moriyama, W. Wang, H. W. Zhang, and J. Q. Xiao: Appl. Phys. Lett. **95** (2009) 122501.
17) P. J. Schuck, D. P. Fromm, A. Sundaramurthy, G. S. Kino, and W. E. Moerner: Phys. Rev. Lett. **94** (2005) 017402.
18) H. Fischer and O. J. F. Martin: Opt. Express **16** (2008) 9144.
19) T. Grosjean, M. Mivelle, F. I. Baida, G. W. Burr, and U. C. Fischer: Nano Lett. **11** (2011) 1009.
20) CONCERTO 7.0 (Vector Fields Ltd., Wimborne, U.K., 2008).